Microchim Acta (2017) 184:1621–1629
DOI 10.1007/s00604-017-2134-2

ORIGINAL PAPER

A Fe_3O_4@SiO_2@graphene quantum dot core-shell structured nanomaterial as a fluorescent probe and for magnetic removal of mercury(II) ion

Mahrouz Alvand [1] · **Farzaneh Shemirani** [1]

Received: 13 September 2016 / Accepted: 16 February 2017 / Published online: 10 March 2017

Abstract The authors describe the synthesis of a multifunctional nanocomposite with an architecture of type Fe_3O_4@SiO_2@graphene quantum dots with an average diameter of about 22 nm. The graphene quantum dots (GQDs) were covalently immobilized on the surface of silica-coated magnetite nanospheres via covalent linkage to surface amino groups. The nanocomposite displays a strong fluorescence (with excitation/emission peaks at 330/420 nm) that is fairly selectively quenched by Hg^{2+} ions, presumably due to nonradiative electron/hole recombination annihilation. Under the optimized experimental conditions, the linear response to Hg^{2+} covers the 0.1 to 70 μM concentration range, with a 30 nM lower detection limit. The high specific surface area and abundant binding sites of the GQDs result in a good adsorption capacity for Hg^{2+} (68 mg·g^{-1}). The material, due to its superparamagnetism, can be separated by using a magnet and also is recyclable with EDTA so that it can be repeatedly used for simultaneous detection and removal of Hg^{2+} from contaminated water.

Keywords Nanocomposite · Adsorption capacity · Fluorescence · Quenching · FTIR · XRD

Electronic supplementary material The online version of this article (doi:10.1007/s00604-017-2134-2) contains supplementary material, which is available to authorized users.

✉ Farzaneh Shemirani
shemiran@khayam.ut.ac.ir

[1] Department of Analytical Chemistry, University College of Science, University of Tehran, P.O. Box 14155-6455, Tehran, Iran

Introduction

Mercury is considered as the most toxic nonradioactive metal, and leads to adverse environmental and health problems such as bioaccumulation by numerous organisms and severe physiological problems, including neurological, neuromuscular, or nephritic disorders originating from its presence in water resources [1]. As a consequence, mercury-indicating methodologies, which are developed to provide critical information for mercury hazard assessment and mercury pollution management, have received much attention. The fluorescence assays display unique advantages of high sensitivity, great simplicity, easy monitoring, and rapid response, providing a better choice for the detection of Hg^{2+} [2]. The typical fluorescent sensing system based on organic dyes exhibits high sensitivity and relative versatility. However, these organic fluorescent probes are mostly synthesized through several steps as well as the structures of the probes are complicated; limit their reliable application in the real sample assay [3]. Therefore, new nanomaterial-based fluorescent probes with a few synthesis steps, high sensitivity and selectivity for Hg^{2+} measurement is of vital importance.

Graphene quantum dots (GQDs), as a member of carbon-based photoluminescent nanomaterial, have increasingly drawn research interests on account of their fascinating physical and chemical properties, chemical inertness, low toxicity, excellent biocompatibility, good dispersibility in water, and stable photoluminescence (PL) [4]. GQDs are graphene nanosheets in the form of one, two or more layers all less than 10 nm thick and 100 nm in lateral size. Compared to graphene sheets with the zero band gap electronic state, GQDs have discrete band-gaps and show typical semiconducting properties [5]. Their band gap and optical properties can be manipulated by reducing their size to nano-level [6]. GQDs are attracting considerable attention as they may gradually replace traditional semiconductor quantum dots due to their superiority in chemical inertness, low toxicity, biocompatibility, high fluorescent activity and excellent photostability [7]. Moreover, compared to the common carbon-based photoluminescent nanomaterials (carbon dots), GQDs exhibit some excellent characteristics such as higher surface area and better surface grafting by using the π–π conjugated network or abundant surface functional groups (carboxyl, hydroxyl, carbonyl, epoxide) [8, 9]. By taking advantages of their unique chemical and optical properties, various GQDs-based fluorescent probes for the detection of metal ions (Fe^{3+}, Cu^{2+}, Pb^{2+} and Hg^{2+}) [10–15], anions (S^{2-}) [16], organic molecules (paranitrophenol) [17] and biomolecules (urea, glucose) [18, 19] have been explored. However, most of these reports have been focused on homogeneous systems as the solution state, which is not recyclable and separable. Since, GQDs have ultrahigh specific surface area due to the nature of nano-sized single layer graphene sheets, they have the potential not only for sensitive detection of pollutants, but also for effective separation and removal of them from environments. It means that novel sensing structures based on GQDs which can firstly detect and then remove pollutants from samples should be developed.

It seems that multifunctional magnetic composite materials, which combines magnetic sorting feature and additional characters from each component, can satisfy above requirement. Fe_3O_4 nanoparticles have been proved promising in site-specific targeting, sample sorting and isolating [20, 21] To improve their performance, Fe_3O_4 nanoparticles are usually covered by silica shell to prevent aggregation and provide sites for surface modification [22].

Bearing the above statement in mind, we synthesized a multifunctional nanocomposite material (Fe_3O_4@SiO_2@GQDs) (Scheme 1). This nanocomposite was successfully prepared by coating of the GQDs onto the surface of amine functionalized Fe_3O_4@SiO_2 nanospheres through acylamide binding in the presence of EDC as the activator. The synthesized nanocomposite exhibited high performance not only for detection, but also the removal of Hg^{2+} from aqueous solution. Additionally, the mercury deposited magnetic nanocomposite can also be recovered and reused without significant loss of its activity. The Fe_3O_4@SiO_2@GQDs nanocomposite was easily separated from solutions by adding an external magnetic field, so the nanospheres with Hg^{2+} were quickly removed. The successful application of the Fe_3O_4@SiO_2@GQDs in the detection of Hg^{2+} ions in real water samples is also demonstrated. The dual application of Fe_3O_4@SiO_2@GQDs as sensing platform and adsorbent can be potentially extended to other environmental systems and biological samples.

Experimental

Reagents

Citric acid, ferric chloride hexahydrate ($FeCl_3.6H_2O$, 97%), ferrous chloride tetrahydrate ($FeCl_2.4H_2O$, 98%), ammonium hydroxide (NH_4OH, 25%), 1-(3-dimethylaminopropyl)3-ethylcarbodiimide hydrochloride (EDC) and $Hg(NO_3)_2.H_2O$, were purchased from Sigma-Aldrich (Chemical Co., Milwauke, WI, USA, www.sigmaaldrich.com). Tetraethyl orthosilicate (TEOS) and 3-aminopropyltriethoxysilane (APTES), was obtained from Merck (Darmstadt, Germany, www.merck.de). 10 mM phosphate buffer solutions were prepared by mixing stock standard solutions of NaH_2PO_4 and Na_2HPO_4. All abovementioned materials were used without any further purification. The deionized water was used in all procedures.

Apparatus

The Fourier transform infrared (FT-IR) spectra of samples were recorded using a Bruker Equinox 55 apparatus (www.bruker.com). Transmission electron microscopy (TEM) was performed using a Zeiss EM10C instrument (www.zeiss.com) at an accelerating voltage of 80 kV. X-ray diffraction (XRD) measurements were carried out using a Bruker, D8-

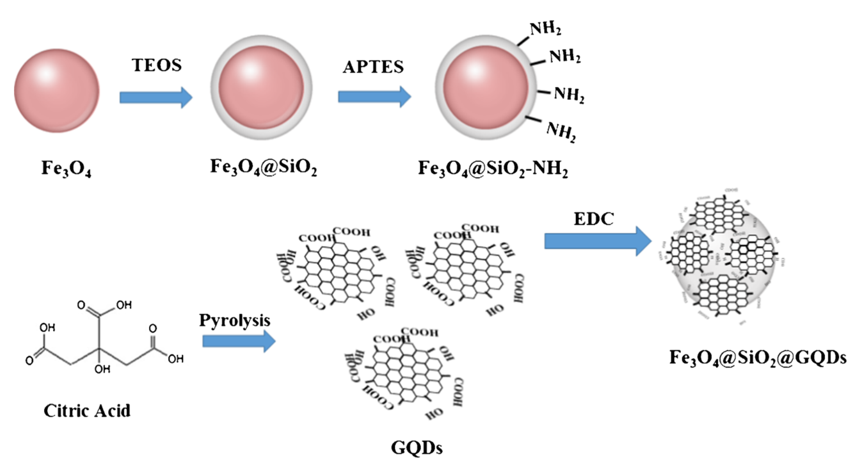

Scheme 1 Illustration for the formation process of Fe_3O_4@SiO_2@GQDs nanocomposite

advance diffractometer (www.bruker.com) with Cu Kα radiation (λ = 1.541874 Å) at a generator voltage of 40 kV and a generator current of 30 mA. Raman spectrum was recorded using an Almega Thermo Nicolet Dispersive Raman Spectrometer (USA) with a 532 nm laser. The magnetic property was analyzed by using a vibrating sample magnetometer (VSM) (Meghnatis Daghigh Kavir Co., Kashan, Iran). Fluorescence spectra were determined by using a Varian Cary Eclipse Fluorescence Spectrometer (www.varianinc.com). Absorption spectrum was determined on a Perkin Elmer, Lambda 25 Spectrophotometer. The concentration of mercury was analyzed by a Varian 710ES Inductively Coupled Plasma Atomic Emission Spectrometry (ICP-AES) (www.varianinc.com).

Preparation of core–shell structured magnetic nanospheres

Synthesis of the GQDs

The GQDs were produced with the use of a simple "bottom-up" method in which citric acid was incompletely pyrolyzed [23]. Briefly, 2 g of citric acid transferred to a 25 mL round bottom flask, and heated to 200 °C by a heating mantle for about 30 min, until the citric acid changed to an orange liquid. This liquid was then dissolved by dropwise addition of a sodium hydroxide solution (10 mg mL^{-1} NaOH) and vigorous stirring until the pH of the GQD solution was neutral (pH = 7.0). This solution was stored at 4 °C.

Synthesis of Fe_3O_4@SiO_2

Fe_3O_4 nanoparticles were synthesized via the co-precipitation of Fe^{2+} and Fe^{3+} ions (molar ratio 1:2) in alkali solution. $FeCl_3.6H_2O$ (3.7 mmol) and $FeCl_2.4H_2O$ (1.85 mmol) were dissolved in 30 mL deionized water and the resulting solution was dropped to a 25% NH_4OH solution (10 mL) with precisely constant drop rate under nitrogen gas and vigorous mechanical stirring (800 rpm) to obtain small and uniform particles. A black precipitate of Fe_3O_4 was continuously stirred for 1 h at room temperature and then heated to 80 °C for 2 h. The synthesized Fe_3O_4 was collected by a permanent magnet after washing three times with deionized water and ethanol. Then, it was dried at 100 °C in vacuum for 24 h. A sample of Fe_3O_4 (1 g) was suspended thoroughly in methanol (80 mL) by ultrasonic bath for 1 h at 40 °C. Then, concentrated ammonia solution was added to the resulting mixture and stirred at 40 °C for 30 min. Afterward, TEOS (1.0 mL) was introduced to the reaction vessel, and continuously stirred at 40 °C for 12 h. The silica-coated magnetic nanoparticles were collected simply in few seconds by a permanent magnet and were thoroughly redispersed and washed with deionized water three times and then dried at 60 °C in vacuum for 24 h.

Preparation of Fe_3O_4@SiO_2@GQDs

For the preparation of Fe_3O_4@SiO_2@GQDs nanocomposites, 0.1 g of the prepared Fe_3O_4@SiO_2 was dispersed in 1.5 mL APTES solution (4% *v*/v in dry toluene). The mixture was stirred under reflux condition at 110 °C for 24 h. After it is cooled to room temperature, the sample was separated from the solution by an external magnet, and washed thoroughly twice with toluene and once with distilled water and the amino-functionalized Fe_3O_4@SiO_2 nanospheres were obtained. Then, the amino-functionalized Fe_3O_4@SiO_2 nanospheres were dispersed in a mixture of 1.0 mL of the prepared GQDs and 1.0 mL of EDC (10 mg mL^{-1}). The mixed suspension was stirred at 4 °C for 12 h. Finally, the Fe_3O_4@SiO_2@GQDs nanocomposites were collected simply in few seconds by a permanent magnet and were thoroughly washed with deionized water to remove unbound GQDs.

General procedure for fluorescent detection

All the fluorescence detections were conducted under the same conditions and the excitation wavelength was set at 330 nm. First, 3 mL phosphate buffered solution of the nanomaterial (4 μg mL^{-1}, pH = 6.0) was added in a quartz cuvette, followed by the addition of a certain volume of Hg^{2+} solution (1×10^{-2} M). The solution was mixed thoroughly and left at room temperature for 1 min for the reaction to complete. The PL spectra of the mixed solutions were recorded and all experiments were performed at room temperature. The concentrations of Hg^{2+} used in the sensitivity experiments were 0, 0.1, 5.0, 10.0, 20.0, 30.0, 40.0, 50.0, 60.0, 70.0, 80.0, 90.0, 100.0, 110.0, 120.0 and 130.0 μM, respectively. 100.0 μM of Hg^{2+} was used in the optimization experiments. Various other metal ions of 100.0 μM were used in the selectivity experiments. The other metal ions used in the selectivity experiments are as follows: Na^+, K^+, Mg^{2+}, Al^{3+}, Cr^{3+}, Ca^{2+}, Mn^{2+}, Ni^{2+}, Fe^{2+}, Fe^{3+}, Pb^{2+}, Cu^{2+}, Co^{2+}, Cd^{2+}, Zn^{2+}.

Adsorption studies

To measure the adsorption kinetics of Hg^{2+} ions onto the Fe_3O_4@SiO_2@GQDs nanocomposite, 10 ml of mercury solution with an initial concentration of 50 mg L^{-1} was introduced into the flask and mixed with 5 mg of Fe_3O_4@SiO_2@GQDs. The solution was stirred continuously at 25 °C. The Hg^{2+} loaded composite nanospheres were then isolated from the solution by adding an external magnetic field at different time intervals. To investigate the equilibrium adsorption isotherms for Hg^{2+}, 5 mg of Fe_3O_4@SiO_2@GQDs was added into 10 mL Hg^{2+} solution with the concentration ranging from 10 to 50 mg L^{-1} and collected until the adsorption equilibrium was reached. The pH values of the above systems were maintained at 6.0. The adsorbent was separated by an external magnetic field. The amount of the target ion in the solution was determined by ICP/AES.

Results and discussion

Structural characterization

Figure 1a, b exhibits the FTIR spectra of GQDs and Fe_3O_4@SiO_2@GQDs nanocomposite. The broad intense peaks at 3300 cm^{-1} are assigned to −OH and −NH groups stretching vibration. Additionally, the peak at 2939 cm^{-1} in spectra shows the asymmetric stretching and symmetric vibrations of C − H. The well-defined peak at 1574 cm^{-1} is related to bending vibrations of C = C group. The peaks at 1668, 1412, and 1049 cm^{-1} were assigned to the C = O, C − O (carboxy), and C − O (alkoxy) functional groups, respectively. For the Fe_3O_4@SiO_2@GQDs nanocomposite (Fig. 1b), the characteristic peak at 1070 cm^{-1} corresponds to the stretching vibration of Si–O and the peak at 583 cm^{-1} is due to the vibrations of Fe–O. The spectrum of the nanocomposite includes the main characteristic peaks of GQDs (beside peaks of Fe_3O_4@SiO_2) that the successful coating of the GQDs onto the surface of Fe_3O_4@SiO_2 nanospheres.

The X-ray diffraction (XRD) patterns of GQDs and Fe_3O_4@SiO_2@GQDs samples are shown in Fig. 1c, d. As shown in Fig. 1c, GQDs exhibited a wide (002) peak at 22.6°, which was in good agreement with the interlayer distance of graphene sheets, demonstrating the graphitic nature of the crystalline dots [24]. The XRD pattern of the Fe_3O_4@SiO_2@GQDs nanocomposite (Fig. 1d) shows diffraction peaks at 2θ = 30.2, 35.5, 43.1, 54.3, 57.1 and 62.8, which can be assigned to the (220), (311), (400), (422), (511) and (440) planes of Fe_3O_4, respectively, indicating that the Fe_3O_4 nanoparticles in the Fe_3O_4@SiO_2@GQDs nanocomposite were pure Fe_3O_4 with a cubic spinel structure; these match well with the standard Fe_3O_4 sample (JCPDS card no. 85–1436). As shown in Fig. 1d, no diffraction peaks corresponding to SiO_2 were observed because the prepared SiO_2 is amorphous. Moreover, no signal about GQDs can be detected, which is explained by the small amounts, high dispersion and low crystallinity of GQDs in Fe_3O_4@SiO_2@GQDs nanocomposite.

Transmission electron microscopy (TEM) was performed to investigate the structure and morphology of the GQDs and Fe_3O_4@SiO_2@GQDs nanocomposite (Fig. 2). From the TEM image (Fig. 2a), it can be seen that the diameters of GQDs were 3–7 nm. Coating of the GQDs onto the surface of Fe_3O_4@SiO_2 nanospheres was achieved through acylamide binding in the presence of EDC as the activator. As shown in Fig. 2b, the resulting composites were spherical nanoparticles with a diameter of about 20 nm and GQDs are present at the periphery of nanospheres.

The magnetic property of the Fe_3O_4@SiO_2@GQDs nanocomposite was investigated by VSM (Fig. S1 (Electronic Supplementary Material, ESM)). The Raman spectrum for the GQDs is shown in Fig. S2 (ESM). More details are placed in the Electronic Supplementary Material (ESM).

Optical characterization

The UV-Vis absorption spectrum of the GQDs showed that there was a shoulder peak at 230 nm and a typical absorption peak at 335 nm (Fig. S3 (ESM)). The peak at 230 nm was attributed to the π-π* transitions of aromatic C = C bonds. The peak at 335 nm corresponds to the n-π* transition of the C = O bond [25]. The fluorescence intensity of Fe_3O_4@SiO_2@GQDs nanocomposite is slightly lower than the free GQDs (Fig. S3 (ESM)).

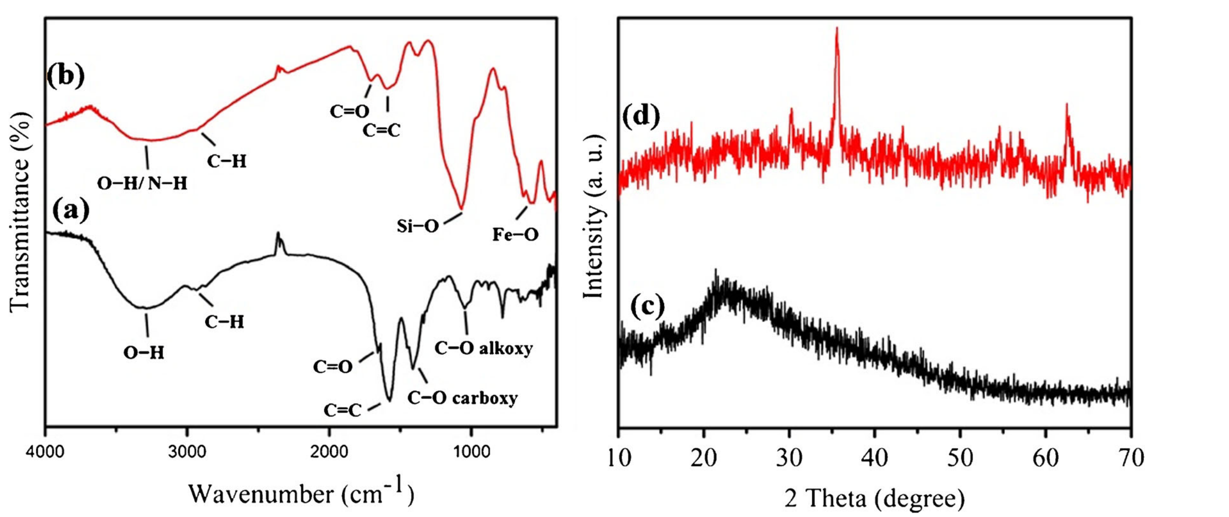

Fig. 1 FTIR spectra of GQDs (**a**) and Fe_3O_4@SiO_2@GQDs nanocomposite (**b**), and XRD pattern of GQDs (**c**) and Fe_3O_4@SiO_2@GQDs nanocomposite (**d**)

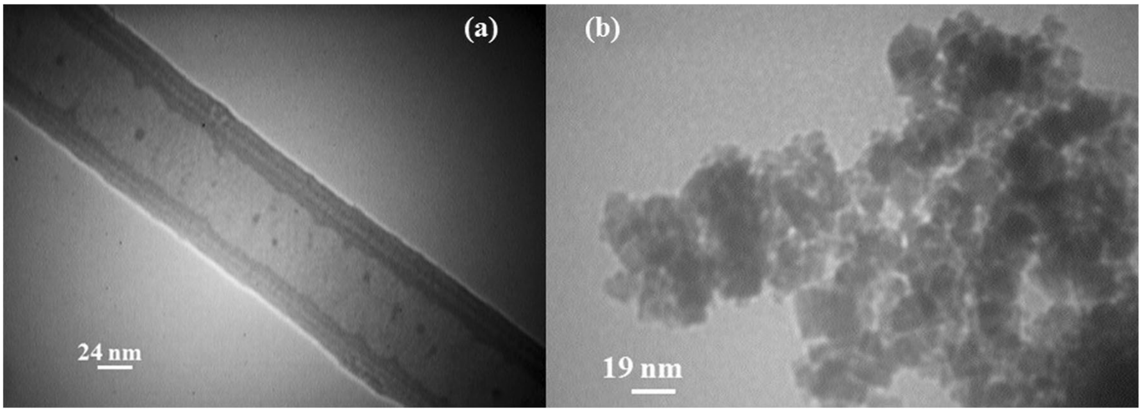

Fig. 2 TEM images of GQDs (**a**) and Fe_3O_4@SiO_2@GQDs (**b**)

The drop in the fluorescence intensity of the nanocomposite can be attributed to the covalent functionalization of the GQDs with silica-coated magnetite nanospheres containing NH_2 groups, which modifies the original moieties in the GQDs. The GQDs aqueous solution exhibited bright blue emission under excitation of 365 nm UV light as shown in Fig. S4a (ESM) inset. The emission wavelength of GQDs is excitation-independent, with the maximum excitation wavelength and the maximum emission wavelength at 335 and 450 nm, respectively (Fig. S4a (ESM)). The excitation-independent emission of the GQDs, implies that both the size and the surface state of those sp^2 clusters contained in GQDs should be uniform, which may contribute to their strong fluorescence emission [23, 26]. In order to confirm that GQDs have been immobilized onto the surface of Fe_3O_4@SiO_2 nanospheres successfully, the fluorescence spectra of Fe_3O_4@SiO_2@GQDs nanocomposite at different excitation wavelengths and photograph under UV light are shown in Fig. S4b (ESM).

Optimization of conditions for Hg^{2+} detection

To improve the performance of the prepared assay for Hg^{2+}, the following parameters were optimized: (a) sample solution pH value; (b) reaction time. Respective data and Figures are given in the Electronic Supplementary Material (ESM). The following experimental conditions were found to give best results: (a) sample solution pH value of 6.0 (Fig. S5, ESM); (b) reaction time of 1 min (Fig. S6, ESM).

Sensitivity of the Fe_3O_4@SiO_2@GQDs for Hg^{2+} detection

The sensitivity of the synthesized Fe_3O_4@SiO_2@GQDs towards the sensing of Hg^{2+} ions was analyzed by fluorescence titrations. From Fig. 3, it can be seen that the fluorescence intensity of Fe_3O_4@SiO_2@GQDs is gradually quenched as the concentration of Hg^{2+} gradually increases from 0 to 130 μM. We found that the fluorescence quenching in this system followed the Stern-Volmer equation [27].

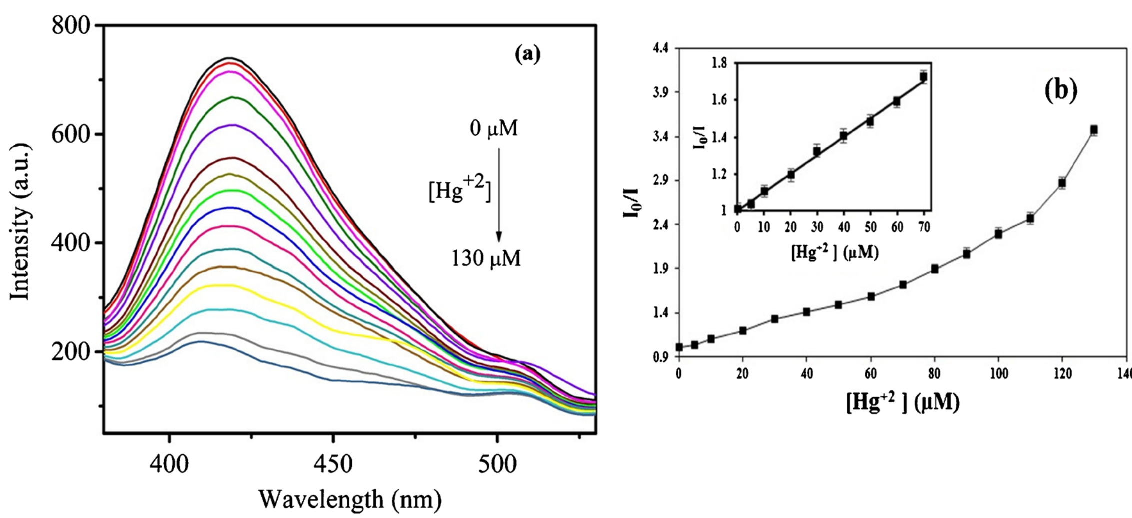

Fig. 3 Emission spectra of the Fe_3O_4@SiO_2@GQDs (4 μg mL^{-1}) in the presence of increasingconcentrations of Hg^{2+} in phosphate buffer (pH = 6.0), excited at 330 nm (**a**) and Stern–Volmer plot for thefluorescence quenching of Fe_3O_4@SiO_2@GQDs by Hg^{2+} ions (inset: linear relationship between I_0/I within the Hg^{2+} concentrations in the range from 0.1 to 70 μM. I_0 and I are the emission fluorescence intensities of Fe_3O_4@SiO_2@GQDs at 420 nm in the absence and presence of metal ions, respectively) (**b**)

$$I_0/I = 1 + K_{SV}[Q] \quad (1)$$

Where I_0 and I are the fluorescence intensity in the absence and presence of Hg^{2+} ions, respectively, K_{SV} is the Stern-Volmer constant, and [Q] is the quencher concentration. Quenching data are usually presented as plots of I_0/I versus [Q]. The Stern-Volmer plot shown in Fig. 3b does not fit a linear calibration plots over the whole Hg^{2+} concentration range of 0.1 to 130 μM. In contrast, inset of Fig. 3b reveals that a linear calibration plot for the quantitative analysis of Hg^{2+} can be fitted between the I_0/I and the concentration of Hg^{2+} at the range from 0.1 to 70 μM, with a linear regression equation of $I_0/I-1 = 0.0101\ [Hg^{2+}] + 0.0006$ (μM) (correlation coefficient $R^2 = 0.996$, $n = 10$). At higher concentrations of Hg^{2+} there is a deviation from linearity (Fig. 3b), probably due to the presence of both static and dynamic mechanisms as observed by other researchers [28]. The error bars represent variations among three separate measurements. The detection limit of 30 nM was obtained based on a 3δ/m (δ is the standard deviation of the blank Fe_3O_4@SiO_2@GQDs sample signal ($n = 10$) and m is the slope of the linear calibration plot), which was lower than most of the previous reported assays for Hg^{2+} detection.

A performance comparison of the methods for the analysis of Hg^{2+} from this work with that from some other studies was investigated (Table 1). It reveals that this method has high sensitivity, good linear response range and comparable detection limit to that found in other studies. The exception are some functionalized semiconductor quantum dots, which are highly sensitive. However, these nanomaterials suffer from intrinsic limitations such as heavy metals potential toxicity and environmental hazards and are being replaced by less toxic nanomaterials such as GQDs and carbon dots.

Selectivity of Fe_3O_4@SiO_2@GQDs for Hg^{2+} detection

To evaluate the selectivity of Fe_3O_4@SiO_2@GQDs for metal ions, the relative fluorescence intensity changes to different metal ions were measured in water (Fig. 4, blue bars). The results indicated that the fluorescence of Fe_3O_4@SiO_2@GQDs was highly quenched by Hg^{2+} and slightly quenched by Fe^{2+} and Fe^{3+} ions, whereas the other tested metal ions induce no obvious changes in the fluorescence intensity ratio. These results clearly demonstrated that the method was highly selective for Hg^{2+} over a number of other metal ions (Fig. 4, blue bar). However, the probe may be unsuitable to use for complicated sample where Fe^{2+} (100 fold) or Fe^{3+} (1000 fold over Hg^{2+}) are exist. Therefore, Fe_3O_4@SiO_2@GQDs can be an efficient probe for Hg^{2+} detection in real water samples with undetectable concentration of Fe^{2+} and Fe^{3+} or after removal of these ions with an appropriate masking agent. Furthermore, competition experiments were conducted in the presence of Hg^{2+} and other metal ions (Fig. 4, green bars). It can be seen that the fluorescence of Fe_3O_4@SiO_2@GQDs upon binding to Hg^{2+} did not significantly change in the presence of other metal ions. The outstanding Hg^{2+} ion selectivity can be ascribed to the strong affinity between Hg^{2+} and the carboxylic (−COOH) and hydroxyl (−OH) functionalities on the GQDs surface over other metal ions as reported in the literature [37]. The selective fluorescence quenching of the nanocomposite by Hg^{2+} is presumably due to the facilitating nonradiative electron/hole recombination annihilation via an effective electron transfer from the GQDs to Hg^{2+} ions [38], i.e. the excited-state electrons transfer to the LUMO of the Hg^{2+} cation from the GQDs, and then, the electrons return to the ground state of the GQDs in a radiationless transfer. Some other metal ions may also adsorb on the surface of GQDs, but the ion binding is weaker and the binding affinity is not as strong as that of Hg^{2+}. Thus, the electron transfer and fluorescence quenching will be weaker [39].

Analytical application

To monitor the possible application of the fluorescence assay for real samples, three different water samples, river water

Table 1 Comparison of the related methods for detection of Hg^{2+}

Materials	Method	Linear range (μM)	LOD (nM)	Ref.
MoS_2 nanosheets	Colorimetric	2–200	500	[29]
Silver@graphene oxide	Colorimetric	10–200	338	[30]
Chitosan-AuNPs	Colorimetric	9–50	1350	[31]
AuNPs@S-C-dots	Colorimetric	0.05–1	47	[32]
Carbon dots	Fluorescence	4–18	2470	[33]
PDDA/CdTe QDs	Fluorescence	0.006–1	5	[34]
Cysteamine/CdTe QDs	Fluorescence	0.006–0.45	4	[35]
Silicon nanocrystals	Fluorescence	0.05–1	50	[36]
Fe_3O_4@SiO_2@GQDs	Fluorescence	0.1–70	30	This work

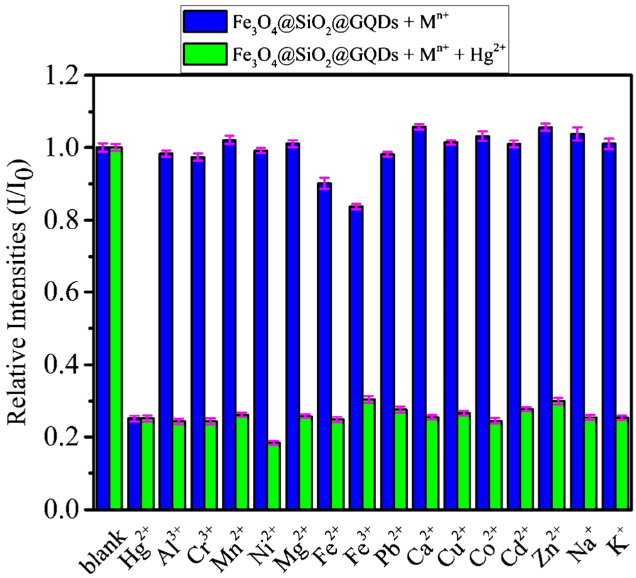

Fig. 4 Selectivity of $Fe_3O_4@SiO_2@GQDs$ (4 μg mL^{-1}) toward Hg^{2+} (100 μM) in the presence of equal amounts of various metal ions

(Babolrud river), well water (Tehran) and tap water (Tehran) were analyzed and the results were summarizes in Table 2. River water was filtered using a 0.45 μm pore size membrane filter to remove suspended particular solids. After dispersing $Fe_3O_4@SiO_2@GQDs$ in each sample, the fluorescence intensity spectra of the prepared samples were recorded to explore possible fluorescence quenching. Table 2 shows the results derived from the recorded fluorescence spectra after the addition of Hg^{2+} with the help of calibration curve. For each sample, five parallel experiments were conducted, and the recoveries from the water samples were excellent and varied from 97.8% to 105.0% with the relative standard deviation (RSD) ranging from 1.2% to 2.2%. These results indicated that the fluorescence analytical assay based on the core–shell $Fe_3O_4@SiO_2@GQDs$ nanospheres has the potential applicability for mercury detection in real samples.

Adsorption performance

Besides the sensing performance, we also investigated the use of the $Fe_3O_4@SiO_2@GQDs$ nanocomposite as an adsorbent for the magnetically guided removal of Hg^{2+} from water samples. The amount of Hg^{2+} adsorption at equilibrium q_e (mg g^{-1}) was calculated by Eq. (2):

$$q_e = \frac{(C_0 - C_e)V}{W} \tag{2}$$

Where C_0 and C_e (mg L^{-1}) are the liquid phase concentrations of Hg^{2+} at initial and equilibrium, respectively, V (L) the volume of the solution, and W (g) is the mass of adsorbent used. Fig. S7 (ESM) shows the adsorption kinetic curve of $Fe_3O_4@SiO_2@GQDs$ to Hg^{2+}. It can be found that the uptake of Hg^{2+} by the nanospheres is a very fast process, which finishes in about 1.5 min. This fast process is attributed to the strong affinity of the fluorescent probe towards Hg^{2+}. To optimize the design of an adsorption system for the adsorption of Hg^{2+}, two equilibrium models, i.e., Langmuir and Freundlich isotherms, have been used to describe the equilibrium characteristics of the adsorption [40]. These adsorption models give a representation of the adsorption equilibrium between the analyte in solution and the active sites of the adsorbent. The Langmuir isotherm is based on the monolayer adsorption model with the homogeneous binding sites on the adsorbent surface. The linear form of Langmuir isotherm can be expressed as;

$$\frac{C_e}{q_e} = \frac{1}{q_{\max} b} + \left(\frac{1}{q_{\max}}\right) C_e \tag{3}$$

Where C_e (mg L^{-1}) is the equilibrium solute concentration, q_e (mg g^{-1}) the equilibrium adsorption capacity, and q_{max} (mg g^{-1}) and b (L mg^{-1}) are Langmuir constants related to maximum monolayer adsorption capacity and energy change in adsorption, respectively. The Langmuir constants q_{max} and b

Table 2 Determination of Hg^{2+} in water samples

Sample	Added (μM)	Found (μM)	Recovery (%)	RSD (n = 5, %)
Tap water	0.0	-	-	-
	2.0	1.97	98.50	1.6
	5.0	5.21	104.2	1.5
	10.0	10.24	102.4	1.2
Well water	0.0	-	-	-
	2.0	2.10	105.0	1.4
	5.0	4.89	97.8	2.2
	10.0	10.12	101.2	1.8
River water	0.0	-	-	-
	2.0	1.98	99.0	2.1
	5.0	5.10	102.0	1.6
	10.0	9.91	99.1	1.3

were calculated from the slope and intercept of the linear plot of C_e/q_e versus C_e, and their values are listed in Table S1 (ESM).

The Freundlich isotherm describes the multilayered adsorption on a heterogeneous surface and is expressed in the linear form as;

$$\ln q_e = \ln k_f + \left(\frac{1}{n}\right)\ln C_e \quad (4)$$

Where K_f and n are the Freundlich constants which represent the adsorption capacity ($mg^{1-1/n}\ L^{1/n}\ g^{-1}$) and adsorption intensity, respectively. K_f and n values were calculated from the intercept and slope of the linear plot between ln q_e and ln C_e, and their values are listed in Table S1. The fit of a model to the experimental data are usually evaluated in terms of linear regression analysis where the R^2 value is used as an indication for the goodness of model fit. With respect to R^2 values (Table S1, ESM), the adsorption of Hg^{2+} on the Fe_3O_4@SiO_2@GQDs can be evaluated as a process that follows the Langmuir model. Therefore, the maximum adsorption capacity of mercury ions is found to be 68.027 mg per gram of Fe_3O_4@SiO_2@GQDs adsorbent.

Recycling sensing performance

An important requirement for the solid multifunctional probe for detection and removal of Hg^{2+} ions is its reusability. To investigate its reusability, 5 mg of Fe_3O_4@SiO_2@GQDs nanosphere was used to complex Hg^{2+} in a repeated adsorption–desorption fashion. In this test, EDTA solution (in deionized water) was used as a stripping agent for removal of Hg^{2+} from the composite nanospheres. Fig. S8 (ESM) indicates the change of fluorescence intensity of Fe_3O_4@SiO_2@GQDs in five repeated experiments. This process involves the following steps: (1) washing Fe_3O_4@SiO_2@GQDs with EDTA (2 mL of 0.01 M EDTA for 5 mg of the nanocomposite) for 2 min, (2) washing Fe_3O_4@SiO_2@GQDs with water and ethanol for 3 times, respectively, (3) fluorescent detection of Hg^{2+}. As shown in Fig. S8 (ESM), the recovered nanospheres was successfully used for at least four consecutive cycles and a very negligible loss of sensing ability was observed (which might be due to the loss of Fe_3O_4@SiO_2@GQDs in the regeneration experiment).

Conclusions

In summary, we designed and synthesized a multifunctional fluorescent probe based on Fe_3O_4@SiO_2@GQDs nanospheres for simultaneously detecting and removing of Hg^{2+}. These multifunctional nanospheres exhibited high selectivity and sensitivity for targeting Hg^{2+} over a number of other metal ions. Since, fluorescence was slightly quenched by Fe^{2+} and Fe^{3+} ions, the Fe_3O_4@SiO_2@GQDs can be an efficient probe for Hg^{2+} detection in real water samples with undetectable concentration of Fe^{2+} and Fe^{3+} or after removal of these ions. Moreover, by the method of ICP-AES, the used nanocomposite proved that they can efficiently remove Hg^{2+} in aqueous solution and be easily separated from the mixture by adding an external magnetic field. More importantly, the Fe_3O_4@SiO_2@GQDs can also be regenerated by treating with EDTA solution and maintain high efficiency upon repeated use for at least four times. This means that the Fe_3O_4@SiO_2@GQDs can be reused and will cause little additional environmental pollution each use compared to the amount of pollution caused by using non-renewable materials. The sensing method has been successfully applied for the detection of Hg^{2+} in real water samples.

Acknowledgements We gratefully acknowledge financial support of this investigation by The Research Council of University of Tehran through Grant (Grant no.94009890).

Compliance with ethical standards The author(s) declare that they have no competing interests.

References

1. Amini MK, Khezri B, Firooz AR (2008) Development of a highly sensitive and selective optical chemical sensor for batch and flow-through determination of mercury ion. Sensors Actuators B Chem 131:470–478
2. Wang ZX, Ding SN (2014) One-pot green synthesis of high quantum yield oxygen-doped, nitrogen-rich, photoluminescent polymer carbon nanoribbons as an effective fluorescent sensing platform for sensitive and selective detection of silver(I) and mercury(II) ions. Anal Chem 86:7436–7445
3. Ding Y, Wang S, Li J, Chen L (2016) Nanomaterial-based optical sensors for mercury ions. Trends Anal Chem 82:175–190
4. Hallaj T, Amjadi M, Manzoori JL, Shokri R (2015) Chemiluminescence reaction of glucose-derived graphene quantum dots with hypochlorite, and its application to the determination of free chlorine. Microchim Acta 182:789–796
5. Li Y, Hu Y, Zhao Y, Shi G, Deng L, Hou Y, Qu L (2011) An electrochemical avenue to green luminescent graphene quantum dots as potential electron-acceptors for photovoltaics. Adv Mater 23:776–780
6. Sun R, Wang Y, Ni Y, Kokot S (2014) Graphene quantum dots and the resonance light scattering technique for trace analysis of phenol in different water samples. Talanta 125:341–346
7. Bacon M, Bradley SJ, Nann T (2014) Graphene quantum dots. Part Part Syst Charact 31:415–428
8. Li L, Wu G, Yang G, Peng J, Zhao J, Zhu JJ (2013) Focusing on luminescent graphene quantum dots: current status and future perspectives. Nanoscale 5:4015–4039
9. Xu J, Wang Y, Hu S (2017) Nanocomposites of graphene and graphene oxides: synthesis, molecular functionalization and application in electrochemical sensors and biosensors. A review. Microchim Acta 184:1–44
10. Zhang C, Cui Y, Song L, Liu X, Hu Z (2016) Microwave assisted one-pot synthesis of graphene quantum dots as highly sensitive

fluorescent probes for detection of iron ions and pH value. Talanta 150:54–60
11. Wang FX, Gu ZY, Lei W, Wang WJ, Xia XF, Hao QL (2014) Graphene quantum dots as a fluorescent sensing platform for highly efficient detection of copper(II) ions. Sensors Actuators B Chem 190:516–522
12. Qi YX, Zhang M, Fu QQ, Liu R, Shi GY (2013) Highly sensitive and selective fluorescent detection of cerebral lead(II) based on graphene quantum dot conjugates. Chem Commun 49:10599–10601
13. Chakraborti H, Sinha S, Ghosh S, Pal SK (2013) Interfacing water soluble nanomaterials with fluorescence chemosensing: graphene quantum dot to detect Hg^{2+} in 100% aqueous solution. Mater Lett 97:78–80
14. Wang B, Zhuo S, Chen L, Zhang Y (2014) Fluorescent graphene quantum dot nanoprobes for the sensitive and selective detection of mercury ions. Spectrochim Acta A Mol Biomol Spectrosc 131: 384–387
15. Li Z, Wang Y, Ni Y, Kokot S (2015) A rapid and label-free dual detection of Hg (II) and cysteine with the use of fluorescence switching of graphene quantum dots. Sensors Actuators B Chem 207:490–497
16. Yu N, Peng H, Xiong H, Wu X, Wang X, Li Y, Chen L (2015) Graphene quantum dots combined with copper(II) ions as a fluorescent probe for turn-on detection of sulfide ions. Microchim Acta 182:2139–2146
17. Zhou Y, Qu ZB, Zeng Y, Zhou T, Shi G (2014) A novel composite of graphene quantum dots and molecularly imprinted polymer for fluorescent detection of paranitrophenol. Biosens Bioelectron 52: 317–323
18. Shao T, Zhang P, Tang L, Zhuo S, Zhu C (2015) Highly sensitive enzymatic determination of urea based on the pH-dependence of the fluorescence of graphene quantum dots. Microchim Acta 182: 1431–1437
19. He YZ, Wang XX, Sun J, Jiao SF, Chen HQ, Gao F, Wang L (2014) Fluorescent blood glucose monitor by hemin-functionalized grapheme quantum dots based sensing system. Anal Chim Acta 810:71–78
20. Xu Y, Zhou Y, Ma W, Wang S, Li S (2013) Functionalized magnetic core–shell Fe_3O_4@SiO_2 nanoparticles for sensitive detection and removal of Hg^{2+}. J Nanopart Res 15:1716–1724
21. Xiao D, Lu T, Zeng R, Bi Y (2016) Preparation and highlighted applications of magnetic microparticles and nanoparticles: a review on recent advances. Microchim Acta 183:2655–2675
22. Lu D, Yang L, Tian Z, Wang L, Zhang J (2012) Core-shell mesoporous silica nanospheres used as Zn^{2+} ratiometric fluorescent sensor and adsorbent. RSC Adv 2:2783–2789
23. Dong Y, Shao J, Chen C, Li H, Wang R, Chi Y, Lin X, Chen G (2012) Blue luminescent graphene quantum dots and graphene oxide prepared by tuning the carbonization degree of citric acid. Carbon 50:4738–4743
24. Liu Y, Liu CY, Zhang ZY (2011) Synthesis and surface photochemistry of graphitized carbon quantum dots. J Colloid Interface Sci 356:416–421
25. Dai Y, Long H, Wang X, Wang Y, Gu Q, Jiang W, Wang Y, Li C, Zeng TH, Sun Y, Zeng J (2014) Versatile graphene quantum dots with tunable nitrogen doping. Part Part Syst Charact 31:597–604
26. Fan LS, Hu YW, Wang X, Zhang LL, Li FH, Han DX, Li ZG, Zhang QX, Wang ZX, Niu L (2012) Fluorescence resonance energy transfer quenching at the surface of graphene quantum dots for ultrasensitive detection of TNT. Talanta 101:192–197
27. Lakowicz JR (2006) Principles of fluorescence spectroscopy. Springer, New York
28. Mohapatra S, Sahu S, Sinha N, Bhutia SK (2015) Synthesis of a carbon-dot-based photoluminescent probe for selective and ultrasensitive detection of Hg^{2+} in water and living cells. Analyst 140: 1221–1228
29. Lu Y, Yu J, Ye W, Yao X, Zhou P, Zhang H, Zhao S, Jia L (2016) Spectrophotometric determination of mercury(II) ions based on their stimulation effect on the peroxidase-like activity of molybdenum disulfide nanosheets. Microchim Acta 183:2481–2489
30. Kamali KZ, Pandikumar A, Jayabal S, Ramaraj R, Lim HN, Ong BH, Bien CSD, Kee YY, Huang NM (2016) Amalgamation based optical and colorimetric sensing of mercury(II) ions with silver@graphene oxide nanocomposite materials. Microchim Acta 183:369–377
31. Chen ZB, Zhang CM, Tan Y, Zhou TH, Ma H, Wan CQ, Lin YQ, Li K (2015) Chitosan-functionalized gold nanoparticles for colorimetric detection of mercury ions based on chelation-induced aggregation. Microchim Acta 182:611–616
32. Shamsipur M, Safavi A, Mohammadpour Z, Ahmadi R (2016) Highly selective aggregation assay for visual detection of mercury ion based on competitive binding of sulfur-doped carbon nanodots to gold nanoparticles and mercury ions. Microchim Acta 183: 2327–2335
33. Yan F, Kong D, Luo Y, Ye Q, He J, Guo X, Chen L (2016) Carbon dots serve as an effective probe for the quantitative determination and for intracellular imaging of mercury(II). Microchim Acta 183: 1611–1618
34. Yang R, Ding X, Zhou Y, Li J, Qu L, Zhang K (2015) A novel fluorescent sensor for mercury (II) ion using self-assembly of poly(diallyl dimethyl ammonium)chloride functionalized CdTe quantum dots. Anal Methods 7:436–442
35. Ding X, Qu L, Yang R, Zhou Y, Yang J, Li J (2015) A highly selective and simple fluorescent sensor for mercury (II) ion detection based on cysteamine-capped CdTe quantum dots synthesized by the reflux method. Luminescence 30:465–471
36. Zhang J, Yu SH (2014) Highly photoluminescent silicon nanocrystals for rapid, label-free and recyclable detection of mercuric ions. Nanoscale 6:4096–4101
37. Lu W, Qin X, Liu S, Chang G, Zhang Y, Luo Y, Asiri AM, Alyoubi AO, Sun X (2012) Economical, green synthesis of fluorescent carbon nanoparticles and their use as probes for sensitive and selective detection of mercury(II) ions. Anal Chem 84:5351–5357
38. Wu ZZ, Li WY, Chen J, Yu C (2014) A graphene quantum dot-based method for the highly sensitive and selective fluorescence turn on detection of biothiols. Talanta 119:538–543
39. Xia YS, Zhu CQ (2008) Use of surface-modified CdTe quantum dots as fluorescent probes in sensing mercury (II). Talanta 75:215–221
40. Foo KY, Hameed BH (2010) Insights into the modeling of adsorption isotherm systems. Chem Eng J 156:2–10